Fast computation of the Narcissus reflection coefficient for the Herschel far-infrared/submillimeter-wave Cassegrain telescope

Robert L. Lucke, Jacqueline Fischer, Arturo M. Polegre, and Douwe A. Beintema

Placement of a scatter cone at the center of the secondary of a Cassegrain telescope greatly reduces Narcissus reflection. To calculate the remaining Narcissus reflection, a time-consuming physical optics code such as GRASP8 is often used to model the effects of reflection and diffraction. Fortunately, the Cassegrain geometry is sufficiently simple that a combination of theoretical analysis and Fourier propagation can yield rapid, accurate results at submillimeter wavelengths. We compare these results with those from GRASP8 for the heterodyne instrument for the far-infrared on the Herschel Space Observatory and confirm the effectiveness of the chosen scatter cone design.
OCIS codes: 070.2580, 260.0260, 260.3090.

1. Introduction

The heterodyne instrument for the far infrared[1] (HIFI) is one of three astronomical instruments currently being fabricated for the Herschel Space Observatory.[2] Herschel, equipped with a passively cooled 3.5 m silicon carbide telescope,[3] is scheduled to be launched to orbit around the second Lagrange point, L_2, of the Earth–Sun system by the European Space Agency in 2007. The HIFI is a spectrometer that is expected to achieve resolving powers up to $R = 10^7$, giving Doppler velocity resolution up to $c/10^7 = 0.03$ km/s. The HIFI covers the frequency range from 480 to 1250 GHz in five bands and the range from 1410 to 1910 GHz in two bands, by use of seven mixers and 14 local oscillator (LO) subbands. Detection sensitivity is expected to be within a factor of 3 of the theoretical quantum noise limit. In addition to the HIFI; Herschel will carry the photodetector array camera and spectrometer[4] (PACS) and the spectral and photometric imaging receiver[5] (SPIRE), together providing imaging and moderate resolution ($100 \leq \nu/\Delta\nu \leq 2000$) spectroscopy over the $55-670$ μm spectral range. Only the HIFI will be considered here.

In a heterodyne detection instrument, some percentage of the mixer noise power leaks out of the feedhorn. Portions of this beam are reflected back by a number of telescope structures, but the secondary mirror (M2, see Figs. 1 and 2) makes by far the largest contribution. M2 is supported by three legs whose surfaces are tilted and beveled to minimize multipath scattering, and other telescope structures are well outside the angle of appreciable acceptance of the feedhorn. To reach the HIFI's expected sensitivity, care must be taken to minimize the effects of Narcissus reflection from M2, some small fraction of which reenters the feedhorn and causes a spectral baseline ripple[6,7] with a period of $\Delta\nu = c/2L \approx 3.6 \times 10^7$ Hz, where c is the speed of light and $L \approx 4.2$ m is the distance between the mixer and the M2. For the HIFI frequency range of $480-1910$ GHz, this period corresponds to velocities of approximately $6-25$ km/s, which means that the baseline ripple, if its amplitude is large enough, can potentially mask, mimic, or distort the Doppler-broadened spectral features that the HIFI is designed to measure.

Although the degrading effects of Narcissus reflection can be alleviated by beam switching, which is done by chopping the optical positions of the HIFI's

R. L. Lucke (lucke@nrl.navy.mil) and J. Fischer are with the U.S. Naval Research Laboratory, 4555 Overlook Avenue, Washington, D.C. 20375-5320. A. M. Polegre is with the European Space Agency, European Space Research and Technology Centre, Antenna and Sub-Millimeter Wave Section, Electromagnetics Division, Keplerlaan 1, PB 299, 2200 AG Noordwijk, The Netherlands. D. A. Beintema is with the SRON Laboratory for Space Research, P.O. Box 800, 9700 AV Groningen, The Netherlands.

Received 14 December 2004; revised manuscript received 13 April 2005; accepted 14 April 2005.
0003-6935/05/285947-09$15.00/0

Report Documentation Page

Form Approved
OMB No. 0704-0188

1. REPORT DATE	2. REPORT TYPE	3. DATES COVERED
2005		**00-00-2005 to 00-00-2005**

4. TITLE AND SUBTITLE	5a. CONTRACT NUMBER
Fast computation of the Narcissus reflection coefficient for the Herschel far-infrared/submillimeter-wave Cassegrain telescope	5b. GRANT NUMBER
	5c. PROGRAM ELEMENT NUMBER
6. AUTHOR(S)	5d. PROJECT NUMBER
	5e. TASK NUMBER
	5f. WORK UNIT NUMBER
7. PERFORMING ORGANIZATION NAME(S) AND ADDRESS(ES) **Naval Research Laboratory,4555 Overlook Avenue, SW,Washington,DC,20375**	8. PERFORMING ORGANIZATION REPORT NUMBER
9. SPONSORING/MONITORING AGENCY NAME(S) AND ADDRESS(ES)	10. SPONSOR/MONITOR'S ACRONYM(S)
	11. SPONSOR/MONITOR'S REPORT NUMBER(S)

12. DISTRIBUTION/AVAILABILITY STATEMENT
Approved for public release; distribution unlimited

13. SUPPLEMENTARY NOTES

14. ABSTRACT

15. SUBJECT TERMS

16. SECURITY CLASSIFICATION OF:			17. LIMITATION OF ABSTRACT	18. NUMBER OF PAGES	19a. NAME OF RESPONSIBLE PERSON
a. REPORT	b. ABSTRACT	c. THIS PAGE			
unclassified	**unclassified**	**unclassified**		**9**	

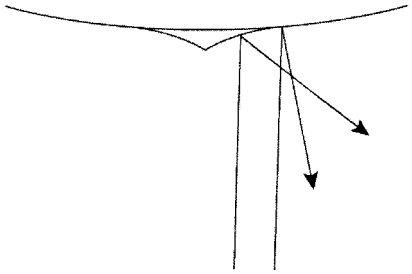

Fig. 1. Schematic geometry of the scatter cone, located at the center of M2. Rays that strike the scatter cone are reflected away from the center of the focal plane.

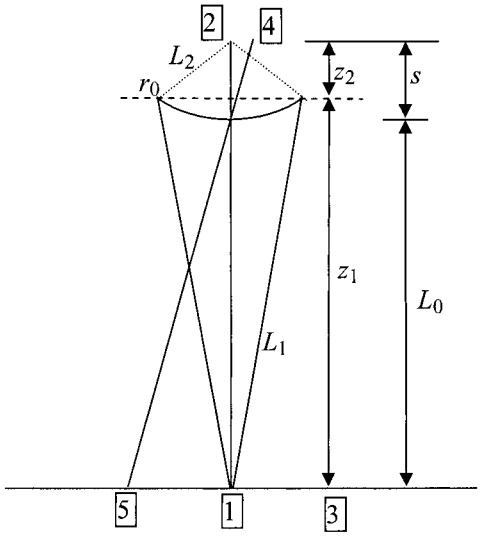

Fig. 2. Geometry of the focal plane and secondary mirror (the scatter cone at the center of M2 is shown in Fig. 1). r_0 is the radius of M2; other dimensions are as shown. A feedhorn at point 1 illuminates the secondary mirror with an 11 dB edge taper and has a virtual image at point 2. A feedhorn at point 3 has a virtual image at point 4 and the center of illumination of the focal plane from this image is at point 5.

Table 2. Allowable Γ_{max} specified for the HIFI

Band	Frequency (GHz)	Γ_{max} (dB)
1	480	−65.0
2	640	−65.8
3	800	−66.6
4	960	−67.4
5	1120	−68.1
5	1250	−68.8
6L	1410	−69.6
6H	1910	−72.0

feedhorns in the telescope's focal plane, or dual-beam switching (nodding), its elimination by design is preferred, since small system changes between beam switches can prevent complete cancellation. The seven HIFI channels are listed in Table 1. Based on measurements of the ripple structure generated by prototype HIFI mixers after reflection of the signal from a flat aluminum plate, and the assumption that measurements will be taken over a time period of 150 s, the maximum allowable power coefficient of reflection for each channel is listed in Table 2.

The power coefficient of reflection Γ is defined as the square of the ratio of the heterodyne signal produced by Narcissus reflection to the signal that would be produced by sending a beam into the feedhorn that exactly matches its output [see Eqs. (5), (9), and (10) below]. Another way to describe the Narcissus effect is with the voltage standing-wave ratio; the relation between them is that the voltage standing-wave ratio equals $(1 + \Gamma^{1/2})/(1 - \Gamma^{1/2})$. Calculating Γ is a problem of long standing[8] and has been addressed in a number of ways, such as various techniques of evaluating the heterodyne detection overlap integral at M2[9–11] or applying the geometric theory of diffraction.[12] Here we report on a different method, based on Fourier

Table 1. Herschel Bands 1–6H[a]

Band	Frequency (GHz)	λ (mm)	w_0 (mm)	X (mm)	Y (mm)	Z (mm)	Γ_{NRL} (dB)	Γ_{G8} (dB)
1	480	0.625	3.89	0	−86	21	−70.0	−70.9
1	640	0.469	2.91	0	−86	21	−72.3	−72.6
2	640	0.469	2.91	0	−57	10	−75.3	−76.7
3	800	0.375	2.33	0	−39	4.6	−89.5	−100.7
4	960	0.312	1.94	±12	−25	2.3	−83.6	−85.1
5	1120	0.268	1.67	0	−12	0.4	−90.9	−96.9
5	1120	0.268	1.67	±12	−12	0.9	−88.9	−94.4
5	1250	0.240	1.49	±12	−12	0.9	−87.6	−92.9
6L	1410	0.213	1.32	0	0	0	−76.8	−83.7
6L	1410	1410	1.32	±12	0	0.4	−88.2	−91.3
6H	1910	0.157	0.98	±12	13	0.5	−89.7	−91.8

[a]The lowest frequency is given for each band except 6H, for which the highest frequency is given. Highest frequencies are also given for bands 1 and 5. w_0 is the beam waist half-diameter at the feedhorn. X, Y, and Z are the coordinates of the center of the feedhorn in the focal plane. X entries labeled ± indicate possible chopping positions. Z is along the optical axis and varies because the focal plane is curved. (Those intimately familiar with Herschel are warned that this is not the convention used by the Herschel program, which interchanges X and Z.) Local maxima in Γ (see text) were calculated by the NRL method and by GRASP8 (G8). The actual value of Γ at a particular frequency depends on how the fringe pattern falls on a feedhorn (see figures) and on the exact distance between the focal plane and the M2.

propagation, that we have developed to calculate Γ for a secondary mirror with a scatter cone.

We model a feedhorn as a Gaussian beam waist in the focal plane of the telescope, but what actually resides in the focal plane is an image of the feedhorn: there are reimaging optics after the focal plane and the real feedhorn resides remotely. (This accounts for the discrepancy the astute reader will observe between the distance from the focal plane to M2, ≈2.7 m, and the distance from the mixer to M2, ≈4.2 m.) We assume that the reimaging optics do not appreciably affect the phase and amplitude structure of the beam to and from the actual feedhorn. The reimaging optics include steering mirrors that alternate the positions of the feedhorn images in the focal plane as they perform the chopping function. We need to assure that the Narcissus reflection coefficient falls below the value specified in Table 2 for all the desired positions.

If M2 had a purely hyperboloidal shape, the computation of Narcissus reflection would be trivial, as shown in Section 2, but its value would well exceed the HIFI specifications. Narcissus reflection is reduced by placing a scatter cone at the center of M2, as shown in Fig. 1. For Herschel, the scatter cone's radial profile is based on the work of Padman and Hills[9]: it is circular with a curvature radius of 450 mm and is tangent to M2's basic hyperboloidal shape at a radius of 16.5 mm. There is a flat spot (not shown in Fig. 1), 1 mm in diameter, at its apex to discourage chipping. The scatter cone reduces Narcissus reflection (as well as unwanted background radiation from high emissivity areas around the telescope's focal plane that would degrade the sensitivity of the PACS and the SPIRE) but makes the reflection much more difficult to calculate.

We will calculate both Γ and the distribution of the reflected radiation in the focal plane so that the effect of changing the location of a feedhorn (while chopping) can be easily visualized. These computations are normally performed by a RF software package such as GRASP8,[13] which solves the problem by physical optics. First, the equivalent currents created by the electromagnetic radiation from the feedhorn that impinges on the surface of M2 are calculated. These currents then radiate into free space and the radiation at a desired point is found by summing all their contributions. The method is time intensive because the surface of M2 must be finely segmented so that the sum converges to an accurate answer. In this paper, the distribution of radiation in the focal plane is found by the superposition-and-Fourier-propagation method described in Section 4, an approach that takes advantage of the simple geometry of the Cassegrain telescope to limit the time-consuming numerical computations to that part of the problem that cannot be solved analytically. This part is the contribution of the scatter cone, and only the scatter cone need be segmented, a fact that drastically reduces the computational part of the problem. Once the amplitude distribution in the focal plane is found, the overlap integral need be evaluated only over the beam waist to find Γ. The result, a complete picture of the illumination of the focal plane and a value for Γ, is obtained in less than 1 min on a 3 GHz computer. Our calculation will be referred to as the NRL (Naval Research Laboratory) calculation to distinguish it from the GRASP8 calculation.

The calculation will be done in stages. First the reflection coefficient is calculated in Section 2 for a large, complete secondary, meaning a purely hyperboloidal mirror with no diameter restriction. Then in Section 3 the focal plane illumination is calculated for a small, complete secondary, meaning the actual diameter is taken into account, and in Section 4 for the actual secondary mirror with the scatter cone. Within this context, large means that the diameter restriction on M2 is removed and complete means that only the hyperboloidal figure is considered (no scatter cone). In Section 5 we present a comparison of the NRL and GRASP8 focal plane illumination calculations. Finally, the Narcissus reflection coefficients of the seven HIFI bands are calculated and discussed in Section 6. The results are summarized in Table 1.

2. On-Axis Reflection Coefficient for a Large, Complete Secondary

We begin with a mathematical description of the electric field of the Gaussian beam emitted by a feedhorn at the beam waist and in the far field at distance z large compared with the Rayleigh distance. The interested reader is referred to Ref. 14 for a thorough introduction to this topic. At the waist, which defines the $z = 0$ reference point in the focal plane, it is

$$E_{G1}(r,\ 0) = E_0 \exp(-r^2/{w_0}^2), \tag{1}$$

where the subscript G denotes Gaussian and 1 denotes the feedhorn, and at distance z it is

$$E_{G1}(r,\ z) = \frac{\pi {w_0}^2}{\lambda z} E_0 \exp\left(-\frac{r^2}{w^2(z)}\right)\exp[i\Phi(r,\ z)], \tag{2}$$

where $w(\Delta z)$ describes the beam width at distance Δz from its waist,

$$w(\Delta z) = \frac{\lambda \Delta z}{\pi w_0}, \tag{3}$$

and $\Phi(r, z)$ is phase. The design of the feedhorns is assumed to be such that $w_0 \propto \lambda$, so $w(\Delta z)$ is independent of λ. At the distance of M2, all the beams have the same diameter, which is $w = 137$ mm. Here $w_0 = 3.89$ mm for 480 GHz. As noted above, $z = 0$ in the focal plane. In Eqs. (2) and (3) z is also the distance from the beam waist, but this will not be true in most of the formulas below.

We need phase, $\Phi(r, z)$, only in the far field, where the wave front is spherical and the Gouy phase shift is constant ($=\pi/2$) and can therefore be ignored. Using $k = 2\pi/\lambda$, we write

$$\Phi(r,\ z) = k\sqrt{r^2 + z^2}. \tag{4}$$

At the beam waist, the LO also has the form of Eq. (1), with E_0 replaced by E_{LO}. If the beam described by Eq. (1) were sent directly back into the feedhorn, then the heterodyne signal that would be produced could be written as

$$\begin{aligned} S_1 &= \int_0^\infty E_{G1}(r,\ 0) E_{\mathrm{LO}} \exp(-r^2/{w_0}^2) 2\pi r \mathrm{d}r \\ &= E_0 E_{\mathrm{LO}} \int_0^\infty \exp(-2r^2/{w_0}^2) 2\pi r \mathrm{d}r \\ &= \frac{\pi}{2} {w_0}^2 E_0 E_{\mathrm{LO}}, \end{aligned} \tag{5}$$

where the upper limit of the integrals is taken as ∞ because the feedhorn is assumed to have negligible beam truncation effects.

We now find the amplitude of the beam returned to the feedhorn by M2, assuming M2 to be large, so that there is no diffraction from its edge, and to have no scatter cone. The geometry of the problem is shown in Fig. 2. M2 is the secondary mirror of a Cassegrain telescope, so it is a hyperboloid that forms a perfect virtual image of the center of the focal plane. Within the useful region of the focal plane, imaging remains essentially perfect, i.e., well within the diffraction limit. The beam produced by reflection from M2 is modeled as coming from this diffraction-limited virtual image of the feedhorn. The distance from the feedhorn to the secondary mirror varies as the location of the feedhorn varies in the focal plane, which is curved (the curvature is not shown in Fig. 2). To have a representative number for use in the following analysis, the on-axis distance $L_0 = 2638$ mm will be used. The vertex radius of the secondary is $R_2 = 345.2$ mm, so the distance s from the vertex to the virtual image of the feedhorn formed by the secondary is given by the imaging equation for a convex reflector:

$$\frac{1}{s} = \frac{1}{L_0} + \frac{2}{R_2} = \frac{1}{2638\ \mathrm{mm}} + \frac{2}{345.2\ \mathrm{mm}} = \frac{1}{162.0\ \mathrm{mm}}. \tag{6}$$

The beam reflected from the secondary is taken to be a Gaussian beam emitted by this virtual image, described at the image by the equivalent of Eq. (1):

$$E_{G2}(r,\ z = L_0 + s) = \frac{E_0}{m} \exp\left[-r^2/(m w_0)^2\right], \tag{7}$$

where $m = s/L_0$ is the magnification, and the reader is reminded that the zero reference point for z is in the focal plane. We must now propagate this beam through the distance $\Delta z = L_0 + s = 2800$ mm back to the feedhorn. We take advantage of the fact that, in the on-axis case, neither the amplitude nor the phase of the beam change appreciably across the feedhorn, so only the field exactly on axis needs to be found. Using the equivalent of Eq. (2) and writing the phase factor in simple form results as

$$\begin{aligned} E_{G2}(0,\ 0) &= \frac{\pi (m w_0)^2}{\lambda (L_0 + s)} \frac{E_0}{m} \exp[i\Phi(0,\ 0)] \\ &= \frac{\pi s {w_0}^2}{\lambda L_0 (L_0 + s)} E_0 \exp[i\Phi(0,\ 0)], \end{aligned} \tag{8}$$

where $\Phi(x, y)$ is the phase in the focal plane. The exact value of Φ depends sensitively on the geometry and the wavelength. We set $\Phi = 0$ to find that the maximum heterodyne signal that can be produced is

$$\begin{aligned} S_2 &= \int_0^\infty E_{G2}(0,\ 0) E_{\mathrm{LO}} \exp(-r^2/{w_0}^2) 2\pi r \mathrm{d}r \\ &= \frac{\pi s {w_0}^2}{\lambda L_0 (L_0 + s)} E_0 E_{\mathrm{LO}} \int_0^\infty \exp(-r^2/{w_0}^2) 2\pi r \mathrm{d}r \\ &= \frac{\pi^2 s {w_0}^4}{\lambda L_0 (L_0 + s)} E_0 E_{\mathrm{LO}}. \end{aligned} \tag{9}$$

We now divide by Eq. (5) and evaluate the result at the HIFI's lowest frequency to obtain the square root of the maximum possible reflection coefficient at this frequency:

$$\begin{aligned} \sqrt{\Gamma} &= \frac{S_2}{S_1} = \frac{2\pi s {w_0}^2}{\lambda L_0 (L_0 + s)} \\ &= \frac{2\pi \times 162 \times 3.89^2}{0.625 \times 2638 \times 2800} = 3.34 \times 10^{-3}, \end{aligned} \tag{10}$$

so $\Gamma = 1.11 \times 10^{-5} = -49.5$ dB at 480 GHz for the ideal on-axis case with a large, complete secondary. Since, as noted below Eq. (3), $w_0 \propto \lambda$, $\Gamma \propto (\mathrm{frequency})^{-2}$.

3. E Field in the Focal Plane for a Small, Complete Secondary

With reference to Fig. 2, the field is modeled, as in Section 2, by use of a virtual image of the feedhorn formed by M2 as the source, then replacing M2 with an aperture of diameter 308 mm in the plane of the mirror's edge. The total sag of M2 is 34 mm and the virtual image is located 162 mm behind M2's vertex, so the plane of M2's edge is $2638 + 34 = 2672$ mm from the center of the focal plane and $162 - 34 = 128$ mm from the virtual image. Thus we have a virtual circular diffracting aperture, illuminated by a virtual on-axis source at distance z_2 (=128 mm), and a real on-axis observation point at distance z_1 (=2672 mm). The solution to this problem is adapted from Eq. (6) of Sommargren and Weaver[15] by using Babinet's principle. The field from the (virtual) source at a point on the other side of the aperture is the sum of the direct

beam from the source and the contribution from diffraction at the rim of the aperture. When the feedhorn is on axis, the result is easily written as

$$E_{\mathrm{CS}}(x,\ y,\ 0) = E_{G2}(x,\ y,\ 0) - E_{G2}(r_0,\ z_1) \times \frac{L_2}{L_1 + L_2} \exp(ikL_1) \times \exp\left(\frac{i\pi r^2}{\lambda L_1}\right) J_0\left(\frac{2\pi r_0 r}{\lambda L_1}\right), \quad (11)$$

where the subscript CS means complete secondary (no scatter cone); x, y, and r are Cartesian and radial coordinates in the focal plane; and the other quantities are given in Fig. 2. The second term is taken from Sommargren and Weaver with (a) obvious changes in notation, (b) their isotropic point source replaced by a Gaussian source; and (c) only the leading term, J_0, kept from an expansion of the Lommel functions. We call the second term the Poisson spot term. Keeping only the J_0 term produces good accuracy in the region near the center of the Poisson spot pattern, which is the only place where the Poisson spot term makes a sizable contribution.

The secondary mirror is illuminated by the Gaussian beam E_{G1}, so the amplitude $|E_{G2}(r_0, z_1)| = |E_{G1}(r_0, z_1)| = (\pi w_0^2/\lambda z_1)\exp[-r_0^2/w^2(z_1)]E_0$ from Eq. (2), and $E_0 = [E_{G2}(0, 0)]\lambda L_0(L_0 + s)/(\pi s w_0^2)$ from Eq. (8), so $|E_{G2}(r_0, z_1)| = |E_{G2}(0, 0)|\ [L_0(L_0 + s)/sz_1] \exp[-r_0^2/w^2(z_1)]$. For the on-axis case, the phase of $E_{G2}(r_0, z_1)$ is ikL_1, so Eq. (11) becomes

$$\begin{aligned} E_{CS}(x,\ y,\ 0) &= E_{G2}(x,\ y,\ 0) - |E_{G2}(0,\ 0,\ 0)|\frac{L_0(L_0 + s)}{sz_1}\frac{L_2}{L_1 + L_2} \times \exp\left(-\frac{r_0^2}{w^2(z_1)}\right)\exp\ 2ikL_1 \times\ \exp\left(\frac{i\pi r^2}{\lambda L_1}\right) J_0\left(\frac{2\pi r_0 r}{\lambda L_1}\right) \\ &= E_{G2}(x,\ y,\ 0) - 0.34|E_{G2}(0,\ 0,\ 0)| \times \exp 2ikL_1 \exp\left(\frac{i\pi r^2}{\lambda L_1}\right) J_0\left(\frac{2\pi r_0 r}{\lambda L_1}\right), \end{aligned} \quad (12)$$

where the Herschel parameters, $r_0 = 154$ mm, $w(z_1) = 137$ mm, $L_0 = 2638$ mm, $L_1 = 2676$ mm, $L_2 = 200$ mm, $s = 162$ mm, $z_1 = 2672$ mm, have been used.

When the feedhorn is off axis; the pattern described by Eq. (12) is shifted off axis, a process that will degrade the approximation because the true off-axis beam will differ somewhat from a shifted on-axis beam. In our calculation, a feedhorn at point 3 in Fig. 2 is imaged at point 4 and an axis drawn from point 4 to point 5 locates the center of the pattern, which is described by Eq. (12) with values of r and $\Phi(r)$ [from Eq. (4)] calculated appropriately for the geometry, that is, using point 5 as the $r = 0$ point. We note in passing that a scatter cone (or similar structure) may sometimes be beneficially placed off center in the secondary if the detector is off center in the focal plane, but such a placement would not be appropriate for Herschel, which has several detectors spread around the focal plane.

4. Effect of the Scatter Cone

The beam leaving the secondary mirror and returning to the focal plane is modeled in the plane of the vertex of M2 as the superposition of E_{G2} from Section 2 and a beam from the scatter cone composed of the negative of E_{G2} plus the beam that is actually produced by the scatter cone:

$$\begin{aligned} E_{\mathrm{RS}}(x,\ y,\ L_0) &= E_{G2}(x,\ y,\ L_0) + [-E_{G2}(x,\ y,\ L_0) + E_{\mathrm{SC}}(x,\ y,\ L_0)]_{r \le r_{\mathrm{SC}}} \\ &\equiv E_{G2}(x,\ y,\ L_0) + E_{\mathrm{FP}}(x,\ y,\ L_0), \end{aligned} \quad (13)$$

where the subscript RS means real secondary, SC means scatter cone, the quantity in brackets is used only for $r \le r_{\mathrm{SC}}$, where r_{SC} is the radius of the scatter cone, the last line defines E_{FP}, and FP means Fourier propagated. Equation (13) correctly describes the beam in the plane of M2's vertex immediately after reflection: outside the scatter cone radius it is $E_{G2}(x, y, L_0)$, within that radius it is $E_{\mathrm{SC}}(x, y, L_0)$. We must find $E_{\mathrm{RS}}(x, y, 0)$, the field in the focal plane. We already know that, when $E_{G2}(x, y, L_0)$ is propagated to the focal plane, the result is $E_{\mathrm{CS}}(x, y, 0)$ from Eq. (12), so we need only propagate the quantity $E_{\mathrm{FP}}(x, y, L_0)$ to the focal plane, i.e., find $E_{\mathrm{FP}}(x, y, 0)$. The secondary is illuminated by $E_{G1}(x, y, L_0)$ from Eq. (2) (suitably evaluated, when needed, for an off-axis feedhorn), and $E_{\mathrm{SC}}(x, y, L_0)$ is found from the phase transformation imposed on this wavefront by the scatter cone, as illustrated (for a lens) in Section 5.1 of Goodman.[16] The sum of $E_{\mathrm{SC}}(x, y, L_0)$ and $-E_{G2}(x, y, L_0)$ is $E_{\mathrm{FP}}(x, y, L_0)$, from which $E_{\mathrm{FP}}(x, y, 0)$ is obtained by Fourier propagation.[16]

The Fourier propagation is performed by filling an $N \times N$ array with zeros except for the central $M \times M$ subarray, which contains the complex field amplitudes that describe $E_{\mathrm{FP}}(x, y, L_0)$ over the area of the scatter cone. For the long-wavelength bands 1–3, $N = 4096$ and $M = 64$. For the short-wavelength bands 4–6, using $N = 8192$ and $M = 128$ results in a slight improvement in accuracy. This array is Fourier transformed, propagated through the distance to the focal plane (the exact propagator is used, not the Fresnel approximation), and inverse transformed to obtain $E_{\mathrm{FP}}(x, y, 0)$, which is added to $E_{\mathrm{CS}}(x, y, 0)$, that is,

$$E_{\mathrm{RS}}(x,\ y,\ 0) = E_{\mathrm{CS}}(x,\ y,\ 0) + E_{\mathrm{FP}}(x,\ y,\ 0). \quad (14)$$

That an $8K \times 8K$ array is needed at the shortest wavelengths of interest points up a fundamental limitation on the Fourier propagation method: the wave-

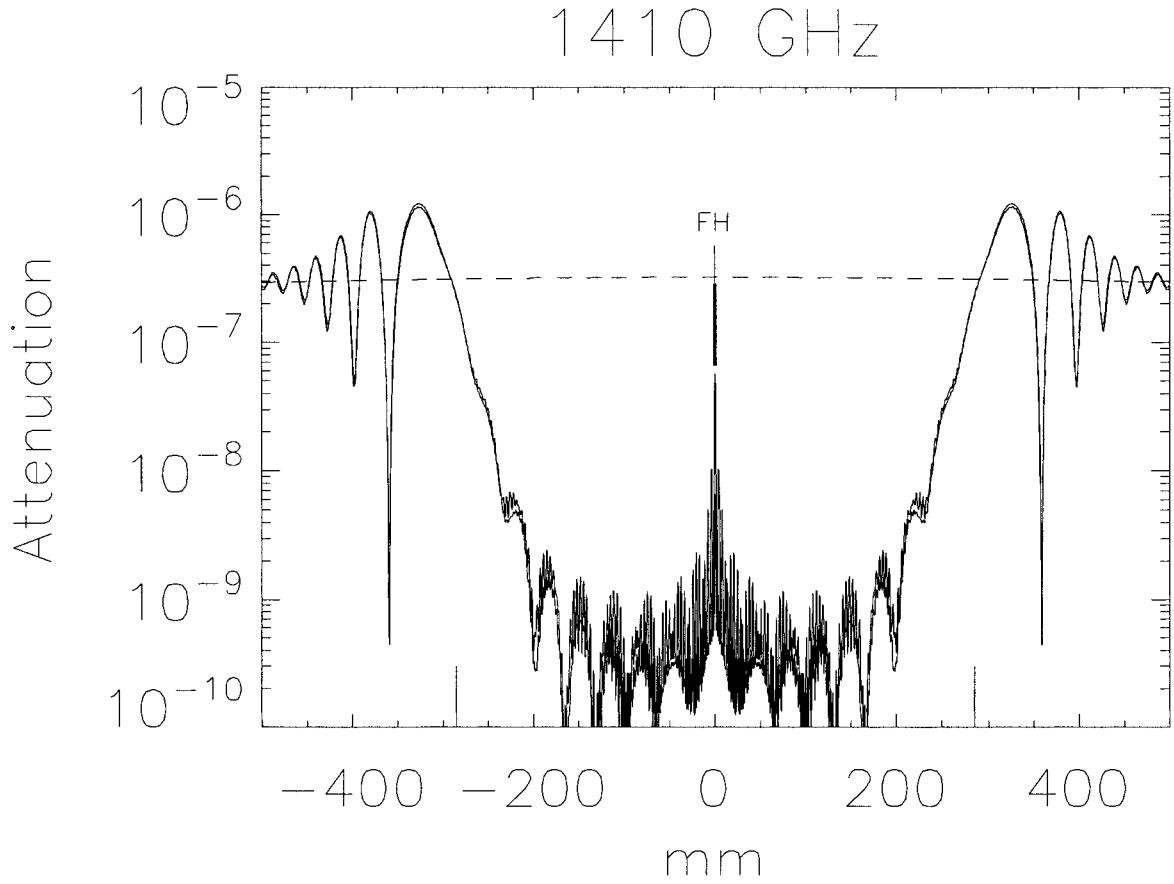

Fig. 3. Two curves show relative intensity, $[E_{RS}(r, 0)/E_0]^2$ = attenuation, in the focal plane for a feedhorn located at the center of the focal plane, obtained by the NRL calculation and by GRASP8. The match between the curves validates the NRL calculation except in the region near the center. The dashed line shows relative intensity, $[E_{G2}(r, 0)/E_0]^2$, for a large, complete secondary (no beam truncation and no scatter cone). The vertical lines marked FH show the center position of the feedhorn and the $\pm w_0$ waist half-diameters. The vertical lines near $\pm$280 mm show the edges of the scatter cone's geometric shadow.

front must be sufficiently densely sampled that the phase change from sample to sample is small compared to 2π (phase sampling errors smaller than $2\pi/14$ are needed for a diffraction-limited calculation), and the width of the area covered by the array must be big enough that, over the desired propagation distance, negligible aliasing occurs. In our case, because the scatter cone is designed to deflect light into a fairly large angle, this requires a width of approximately 2 m for the propagation distance of nearly 3 m. When $M = 128$ is used to cover the 33 mm scatter cone, one pixel = $33/128 \approx 0.25$ mm, and an $8K \times 8K$ array is needed to cover a 2 m square. Performing the same computation at shorter wavelengths would quickly become impossible.

5. Focal Plane Illumination and Comparison with GRASP8

Figure 3 shows the NRL and the GRASP8 calculations of the focal plane illumination at 1410 GHz, chosen because band 6L is the only one for which the feedhorn can be exactly on axis. Relative intensity is plotted along a diameter that passes through the center of the focal plane. The two curves show excellent agreement near the edge of the geometric shadow of the scatter cone and outside it. The region near the center of the shadow is shown in finer detail in Fig. 4. In this region, the NRL calculation has a higher average level and shows much larger rapid intensity oscillations than does GRASP8. This interference structure comes from the Poisson spot term of Eq. (12). At the exact center, the NRL value is approximately 6×10^{-8}, and the GRASP8 value is approximately 7×10^{-9} (the reader is reminded that the calculations give amplitudes that are squared to yield intensities, so the calculated amplitudes at the center differ by a factor of $\approx$3). We are not certain what accounts for the discrepancy between the NRL and the GRASP8 results shown in Figs. 3 and 4. The primary difference is in the Poisson spot term, and we note that the NRL calculation is for a scalar wave, while GRASP8 includes polarization. This may account for at least some of the difference in reflection from the rim of M2. We suggest that comparing the results of GRASP8 to a theoretical calculation of Poisson's spot in simpler geometry than we have here (say, a plane wave impinging on a flat plate) would be a good project for an interested party to address.

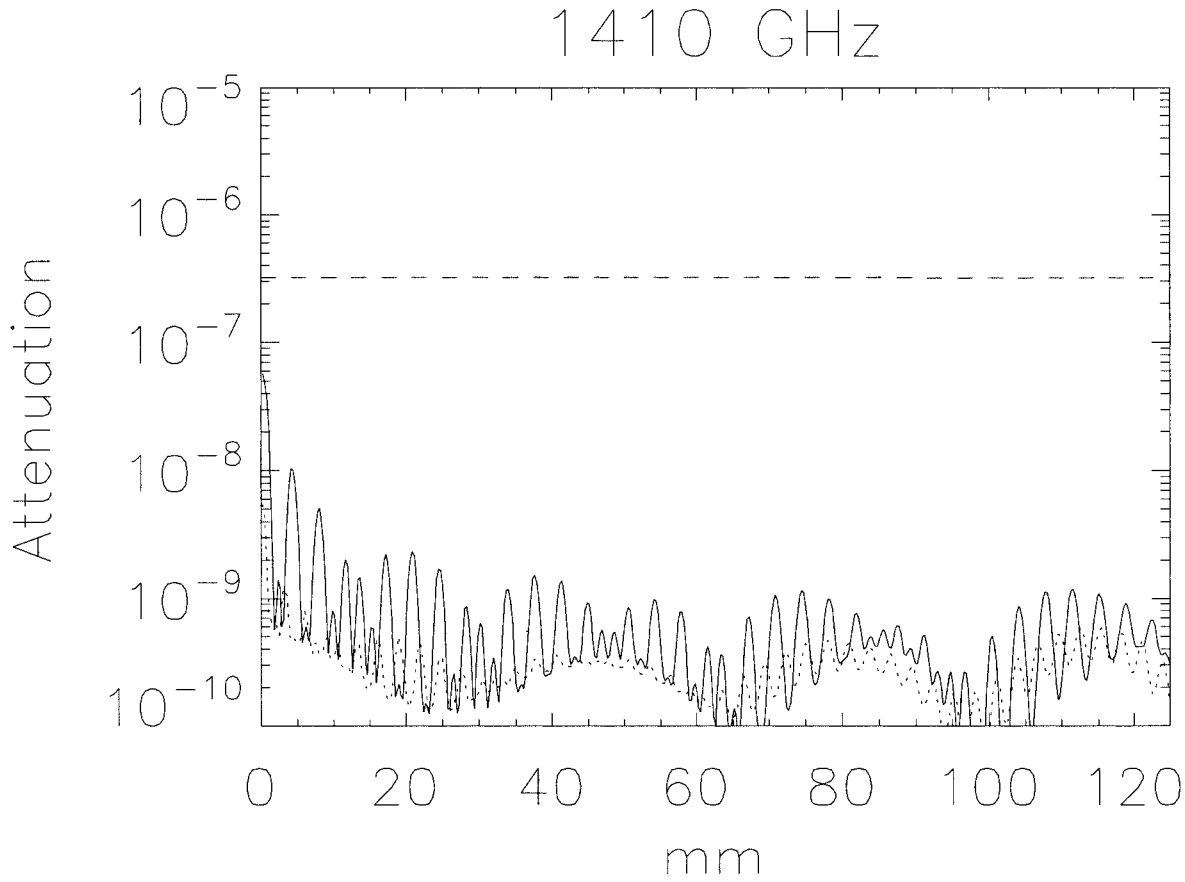

Fig. 4. Details of Fig. 3. The solid curve shows the NRL calculation, the dotted curve that of GRASP8. In this region, the NRL calculation has a higher average level and much larger oscillations than GRASP8.

Figure 5 shows the comparison between the NRL and the GRASP8 at 480 GHz, with the feedhorn located 84 mm from the center of the focal plane. The center of the figure is the center of the focal plane, and the relative intensity is plotted along a line that passes through the center of the focal plane and the center of the feedhorn. Once again there is good agreement between the calculations near and outside the geometric shadow of the scatter cone, and in this case the match is also fairly good at the center of the Poisson spot pattern (i.e., at -84 mm, where the value is approximately 6×10^{-7} for NRL, approximately 4×10^{-7} for GRASP8), but again the NRL calculation shows much larger intensity oscillations.

The plane of Figs. 3–5 is nominally the Y axis in Table 1, that is, it passes through the nominal, unchopped position of the feedhorn. In the chopped position, the image of the feedhorn is moved as much as 12 mm in the $\pm X$ direction. Since the feedhorn is the source of the pattern, as far as the figures are concerned the only effect of chopping is to move the feedhorn radially by a small amount. For channel 1, the feedhorn moves from 84 mm to $(84^2 + 12^2)^{1/2} \approx 85$ mm, a negligible amount. Bands 4–6 are close enough to the center of the focal plane for the 12 mm change in the X direction to affect their radial distance materially, and chopped positions are shown in Table 1 for these bands. In band 6L, moving the feedhorn to a 12 mm off-axis position moves the Poisson spot pattern 12 mm in the opposite direction. This separates the feedhorn from the Poisson spot maximum by 24 mm and, as can be inferred from Fig. 3 and as stated explicitly in Table 1, greatly reduces the reflection coefficient.

6. Reflection Coefficients

Once $E_{\mathrm{RS}}(x, y, 0)$ is found, the integral in Eq. (9) is performed numerically [with E_{G2}, which is real in Eq. (9), replaced by E_{RS}, which is complex] and the magnitude of the ratio in Eq. (10) is squared to find the reflection coefficient. Figures 3–5 show fringe patterns produced in the focal plane and, consequently, the difference in attenuation that can result from a slightly different placement of a feedhorn. Thus, for example, slightly different chopping positions can result in somewhat different values of the reflection coefficient. The same is true of different wavelengths within a band: the fringe pattern scales with wavelength, so a change in wavelength has an effect similar to a change in feedhorn position. In evaluating Γ, therefore, we have slightly varied the radial position (never by more than 2 mm) from the nominal Herschel specification to obtain a local maximum in Γ.

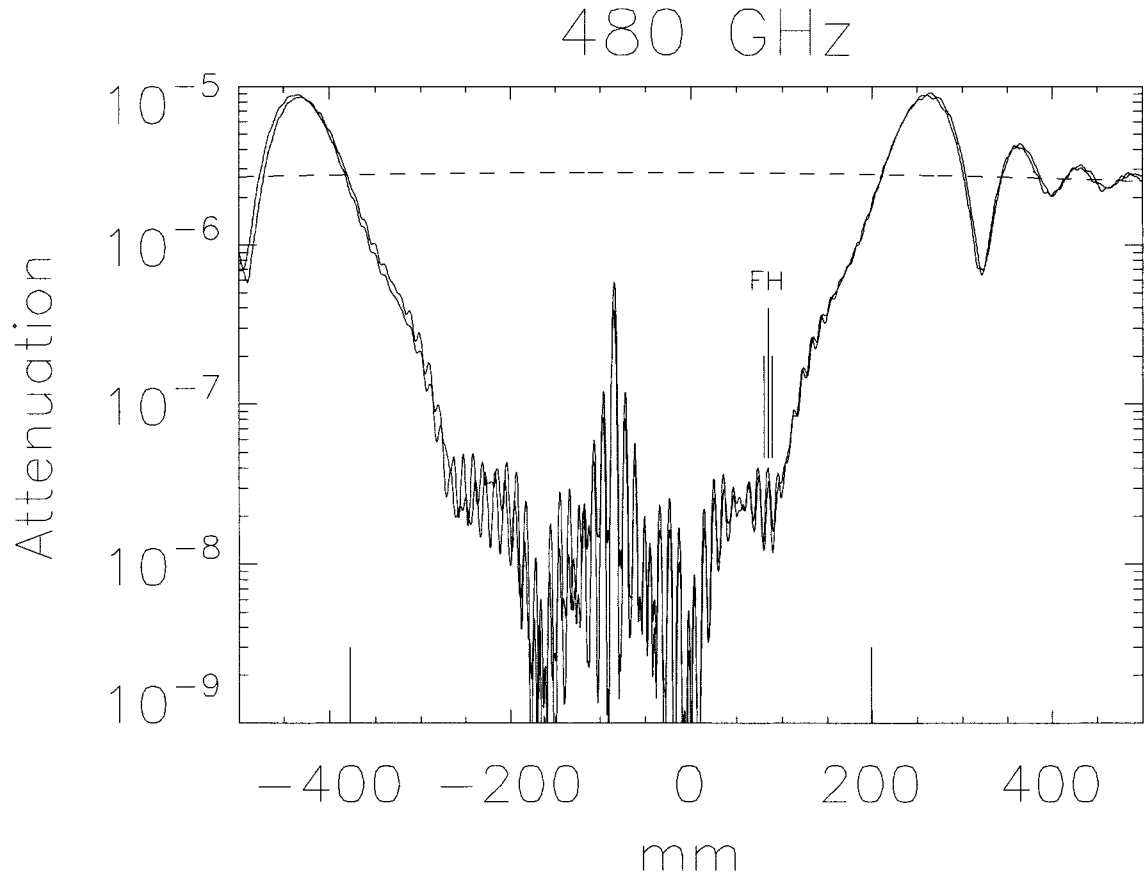

Fig. 5. Comparison of the NRL calculation and GRASP8 at 480 GHz and feedhorn 84 mm from the center of the focal plane. The NRL calculation has larger oscillations in the geometric shadow of the scatter cone than does GRASP8.

Results are given in Table 1 for these positions using both the NRL and the GRASP8 calculations.

Table 1 shows that the disagreement between the NRL and the GRASP8 calculations of illumination discussed in Section 5 becomes, for the on-axis 1410 GHz case, a disagreement on Γ. The NRL value is −76.8 dB, whereas GRASP8 gives −83.7 dB. Unlike the other cases, which are all off axis, the on-axis case can also be evaluated with reasonable efficiency by executing the heterodyne detection overlap integral at the surface of M2.[9] One of us (D. A. Beintema) performed this computation and obtained a result of −79.7 dB. The difference between NRL and GRASP8 is 6.9 dB, which is a factor of 4.9 in Γ or 2.2 in $\Gamma^{1/2}$. The reader is reminded that it is the latter that is calculated directly, then squared to yield the former. The factor of 2.2 difference in $\Gamma^{1/2}$ is less than the factor of 3 difference in amplitude cited in Section 5 because the phase of the Poisson spot term varies across the feedhorn, so it contributes less to $\Gamma^{1/2}$ than do the other components of $E_{RS}(x, y, 0)$ [see Eq. (14)], which are essentially constant across the feedhorn. Thus, the differences among the three calculations need not be regarded as large, especially considering that the fields calculated are in the geometric shadow, where the field is the sum of three large contributions whose vector sum is close to zero: that of M2, that of the scatter cone, and that of Poisson's spot. It takes only relatively small errors in the values of these large terms to cause a substantial error in their sum.

In Table 1 we note that 480 GHz in band 1 has the largest Γ, mostly because it is close enough to the edge of the geometric shadow of the scatter cone, as shown in Fig. 5, to receive a substantial amount of radiation diffracted into the shadow. The 640 GHz in band 1 has a lower Γ because its shorter wavelength results in a sharper shadow edge. Γ is lower still for 640 GHz in band 2 because the band 2 feedhorn is farther from the edge. Frequencies of 800 GHz and higher fall well inside the shadow of the scatter cone and Γ is dominated by diffraction from the outer edge of the mirror, i.e., by the Poisson spot term in Eq. (12). The Γ values at higher frequencies are generally around −90 dB except for the special case of 1410 GHz in the on-axis (unchopped) position, which is much higher because its central position causes it to be exposed to the maximum of the pattern, i.e., to Poisson's spot itself. As discussed in Section 5, the disagreement between the NRL calculation and the GRASP8 is maximal at this point, but even the higher NRL calculation shows the reflection coefficient to be below the specification in Table 2. Table 2 gives the maximum allowable values of Γ specified by

the HIFI. All the calculated values in Table 1 are well below the specifications: the design of the scatter cone meets its performance criteria.

7. Conclusion

A hybrid analytical–numerical method for calculating Narcissus reflection at submillimeter wavelengths for the simple geometry of a small scatter cone on the secondary mirror of a Cassegrain telescope has been described. The method has been validated by comparison to the results of the GRASP8 physical optics code and has verified the theoretical performance of the Herschel scatter cone, as shown in Table 1 and Figs. 3–5. The method has the advantage of speed. For example, it generated Fig. 3 and the corresponding reflection coefficient in Table 1 in less than 1 min on a 3 GHz computer. GRASP8 required approximately 1.5 h and 12 min, respectively, on a 2.2 GHz machine.

We suggest that polarization-dependent reflection from the rim of M2 may be responsible, at least in part, for the discrepancies shown in Figs. 3–5 between the NRL and the GRASP8 calculations, and we recommend further investigation of this point to any interested party.

We gratefully acknowledge helpful discussions with Tom Phillips (California Institute of Technology), Nick Whyborn (SRON), and Peter Gaiser (NRL). R. Lucke and J. Fischer acknowledge support from the U.S. Office of Naval Research and the National Aeronautics and Space Administration's Herschel Project Office at the Jet Propulsion Laboratory of the California Institute of Technology.

References

1. Th. De Graauw, F. P. Helmich, "Herschel-HIFI: the heterodyne instrument for the far-infrared," in *The Promise of the Herschel Space Observatory*, G. L. Pilbratt, J. Cernicharo, A. M. Heras, T. Prusti, and R. Harris, eds., **SP-460,** 45–51 (European Space Agency, 2001).
2. G. L. Pilbratt, "Herschel Space Observatory mission overview," in *IR Space Telescopes and Instruments*, J. C. Mather, ed., Proc. SPIE **4850,** 586–597 (2003).
3. E. Sein, Y. Toulemont, F. Safa, M. Duran, P. Deny, D. de Chambure, T. Passvogel, and G. L. Pilbratt, "A Φ3.5m SiC telescope for Herschel mission," in *IR Space Telescopes and Instruments*, J. C. Mather, ed., Proc. SPIE **4850,** 606–618 (2003).
4. A. Poglitsch, C. Waelkens, and N. Geis, "The Photodetector Array Camera and Spectrometer (PACS) for the Herschel Space Observatory," in *IR Space Telescopes and Instruments*, J. C. Mather, ed., Proc. SPIE **4850,** 662–673 (2003).
5. M. J. Griffin, B. M. Swinyard, and L. G. Vigroux, "SPIRE—Herschel's Submillimetre Camera and Spectrometer," in *IR Space Telescopes and Instruments*, J. C. Mather, ed., Proc. SPIE **4850,** 686–697 (2003).
6. R. J. Allen, "The radio spectrum of Virgo A from 1411.7 to 1423.8 MHz," Astron. Astrophys. **3,** 316–322 (1969).
7. D. Morris, "Chromatism in radio telescopes due to blockage and feed scattering," Astron. Astrophys. **67,** 221–228 (1978).
8. S. Silver, *Microwave Antenna Theory and Design* (McGraw-Hill, 1949); reprinted by Peter Peregrinus, London, in 1984 as Vol. 19 of the IEEE Electromagnetic Waves Series).
9. R. Padman and R. E. Hills, "VSWR reduction for large millimeter-wave cassegrain radiotelescopes," Int. J. Infrared Millim. Waves **12,** 589–599 (1991).
10. G. T. Poulton and S. H. Lim, "Calculation of input-voltage standing-wave ratio for a reflector antenna," Electron. Lett. **8,** 610–611 (1972).
11. C. Dragone and D. C. Hogg, "The radiation pattern and impedance of offset and symmetrical near-field Cassegrainian and Gregorian antennas," IEEE Trans. Antennas Propag. **AP-22,** 472–475 (1974).
12. A. R. Lopez, "The geometrical theory of diffraction applied to antenna pattern and impedance calculations," IEEE Trans. Antennas Propag. **AP-14,** 40–45 (1966).
13. K. Pontopiddan, ed., *Technical Description of GRASP8*, (TICRA Engineering Consultants, 2002), ISBN 87-989218-0-0, Sec. 2.3.1.3.
14. P. F. Goldsmith, *Quasioptical Systems; Gaussian Beam Quasioptical Propagation and Applications* (Institute of Electrical and Electronics Engineers, 1998).
15. G. E. Sommargren and H. J. Weaver, "Diffraction of light by an opaque sphere. 1: Description and properties of the diffraction pattern," Appl. Opt. **29,** 4646–4657 (1990).
16. J. W. Goodman, *Introduction to Fourier Optics* (Wiley 1968), Secs. 3.7 and 5.1.